Search for instability-induced amorphization in deuterated $ErFe_2$

C. E. Krill III* and J. Li
W. M. Keck Laboratory of Engineering Materials 138-78, California Institute of Technology, Pasadena, California 91125

W. B. Yelon
University of Missouri Research Reactor and Department of Physics, University of Missouri-Columbia, Columbia, Missouri 65211

W. L. Johnson
W. M. Keck Laboratory of Engineering Materials 138-78, California Institute of Technology, Pasadena, California 91125
(Received 15 March 1993)

Experimental evidence—in the form of a specific-heat anomaly—for instability-induced amorphization of $ErFe_2$ by hydrogenation was recently reported by Fecht, Fu, and Johnson [Phys. Rev. Lett. **64**, 1753 (1990)]. We have attempted to study this anomaly by *in situ* elastic neutron diffraction and differential-scanning-calorimetry (DSC) measurements of deuterated $ErFe_2$ below and above the reversible, endothermic, λ-shaped enthalpy signal that they found at $\sim 200\,^{\circ}C$. Our combined diffraction and DSC results reveal that the amorphization transition is irreversible, strongly exothermic and occurs only at a significantly higher temperature than that of the specific-heat anomaly. Rather than resulting from an underlying instability of the crystalline phase, amorphization occurs as a by-product of short-range clustering of the Er and Fe atoms, which is driven by the creation of energetically more favorable sites for the deuterium atoms.

I. INTRODUCTION

Amorphization transformations can be induced in solids by a variety of experimental techniques, such as hydrogenation, interdiffusion reactions, irradiation, implantation, high-energy milling, and the application of pressure.[1] In most of these cases, the amorphous phase is known to nucleate heterogeneously at dislocations, grain boundaries, antiphase domain boundaries, and free surfaces.[1-4] In light of several recent experimental results, however, it has been proposed that amorphization might occur *homogeneously* under certain experimental conditions: namely, those in which the crystalline phase is driven toward an intrinsic instability at which it collapses to the amorphous state. Experimental support for such a conjecture comes from observations of electron irradiation-induced amorphization of Cu_4Ti_3,[5] measurements of shear modulus attenuation in irradiated intermetallic thin films,[6] measurements of critical strain[7] and atomic mean-square displacements[8,9] preceding amorphization of supersaturated alloys, and computer simulations of binary Lennard-Jones alloys.[10]

Fecht and Johnson have developed a general polymorphous phase diagram for crystals that predicts instability-induced amorphization to occur when enough "defects" are pumped into the crystal.[11,12] These "defects" can be of the usual sort (vacancies, dislocations, or grain boundaries) or more generalized, such as the internal strain fields resulting from interstitial incorporation of atoms or substitutional alloying by atoms of a different size. As long as the crystal is constrained to remain in its original phase (that is, phase separation is suppressed), Fecht and Johnson demonstrated that there must exist an upper concentration limit of "defects" that the crystal can incorporate without catastrophically falling apart into a liquid or amorphous phase.

Hydrogenation is a promising method for testing this idea because hydrogen atoms can diffuse into many metals at temperatures too low for the much heavier metal atoms to move, thus enabling the hydrogen atoms to act as "defects" without causing phase separation or structural transformation, at least at low hydrogen concentrations. The small size of H atoms permits them to occupy interstitial sites in the metal lattice, but not without inducing some volume expansion; the energy needed to expand the lattice is derived from the energy gained from metal-hydrogen bonds. Above a certain hydrogen concentration, however, the lattice can no longer tolerate the increased volume necessary to incorporate the additional hydrogen atoms; consequently, it transforms to another structure or separates into multiple phases. Sometimes, the result is a uniformly amorphous phase, as first demonstrated convincingly in 1983 by Yeh, Samwer, and Johnson.[2] They observed the gradual disappearance of Bragg peaks in x-ray-diffraction scans of melt-spun crystalline ribbons of Zr_3Rh annealed in 1×10^5 Pa (1 atm) of hydrogen at $\sim 180\,^{\circ}C$. The radial distribution function of the amorphous Zr_3Rh hydride formed by this process was essentially identical to that of a sample made by hydrogenating an already-amorphous ribbon of Zr_3Rh made by rapid quenching, thus supporting the contention that the loss of Bragg peaks corresponded to a true loss of crystalline order.[13]

Subsequently, hydrogen-induced amorphization (HIA) was observed in a wide variety of intermetallic compounds of the form $A_{1-x}B_x$, where A is a hydride-forming metal and B is a nonhydride-forming metal.[14] Upon being annealed in a hydrogen atmosphere, many of these intermetallics transform directly from the crystalline state to the amorphous state, while some others first pass through an intermediate crystalline hydride state before becoming amorphous.[15,16] $ErFe_2$ is a member of the

latter class of compounds: upon being heated in a hydrogen atmosphere, $ErFe_2$ transforms to a crystalline hydride at $\sim 50\,^{\circ}C$ and then to an amorphous phase at $\sim 220\,^{\circ}C$.[15,17] According to the Fecht-Johnson argument,[11] the amorphization of such a crystalline hydride could be thought of as a polymorphous phase transition (analogous to melting in that long-range order is lost) occurring in response to an underlying instability of the crystalline lattice, if it were not for the fact that the amorphous product phase actually has *less* hydrogen (~ 2.8 H atoms per $ErFe_2$ formula unit) than the crystalline hydride starting material (~ 3.2 H per $ErFe_2$). If the hydrogen content could be kept constant through the transition, however, it should be possible to observe instability-induced amorphization of $ErFe_2$ hydride, as predicted by Fecht and Johnson's theory.

It was this latter idea that motivated Fecht, Fu, and Johnson[17] to perform a differential-scanning-calorimetric (DSC) study of hydrogen-induced amorphization of $ErFe_2$. They placed a small amount of the crystalline hydride in a sealed capsule (to maintain a constant hydrogen concentration) and measured the enthalpy change upon heating in the DSC. To their surprise, they observed an unusual λ-shaped endothermic signal at $\sim 200\,^{\circ}C$ that seemed to be at least partially reversible. Analysis of the sample by transmission electron microscopy after cooling back to room temperature revealed the presence of amorphous regions, suggesting that this so-called "λ anomaly" is associated with an amorphization transformation of the crystalline hydride. This claim led us to devise experiments enabling *in situ* observation of the structure of the hydride both below and above the anomaly; our results—while not confirming those of Fecht, Fu, and Johnson—shed some light on the mechanism of hydrogen-induced amorphization and on the assumptions implicit in the polymorphous phase diagram of Fecht and Johnson.

II. EXPERIMENTAL PROCEDURES

Ingots of $ErFe_2$ weighing ~ 5 g were prepared from sublimed, dendritic Er lump (REacton grade, 99.99%) and vacuum-remelted, low-oxygen Fe lump (REacton grade, 99.99%). Stoichiometric amounts were alloyed by induction melting in an argon atmosphere, the process being repeated at least three times to improve homogeneity. Each ingot was then sealed in helium with a titanium getter and annealed at $\sim 850\,^{\circ}C$ for at least 2 days, causing the $ErFe_2$ grain size to grow to a typical diameter of $\gtrsim 200\ \mu m$. The ingot was subsequently ground into a fine powder and sifted through a No. 325-mesh ($< 44\ \mu m$) screen in order to create a majority of single-crystalline particles, thus removing grain boundaries as potential heterogeneous nucleation sites for amorphization. Formation of the crystalline deuteride was accomplished by annealing the powder in an atmosphere of deuterium (C.P. grade 99.5% or research grade 99.99%) at a pressure of 5.9×10^5 Pa (85 psi). The initial annealing temperature of 180–200 °C was maintained for at least 8 h and then lowered slowly to room temperature. Uptake of deuterium was observed to occur very quickly, often even at room temperature. Chemical analysis of the deuterium concentration in samples prepared by this procedure found ~ 3.2 D atoms per $ErFe_2$ formula unit.

X-ray diffraction was used to characterize the $ErFe_2$ powder before and after deuteration. Diffraction scans were obtained from an INEL 120° (2θ) position-sensitive detector mounted in Debye-Scherrer geometry with monochromated Co-$K\alpha$ radiation [$\lambda = 0.179\,03$ nm (Ref. 18)]. The powder samples were mounted on glass slides and held at a fixed incidence angle of $\sim 15°$. Bragg peaks from both $ErFe_2$ and $ErFe_2D_{3.2}$ were very sharp, confirming the presence of large grains. Splitting of the C15 diffraction peaks in the diffraction scan of $ErFe_2D_{3.2}$ indicate that its room-temperature structure is a rhombohedral distortion of the cubic lattice of $ErFe_2$. This distortion is consistent with that found in $ErFe_2H_x$ for $3.2 \lesssim x \lesssim 3.6$ (Refs. 19 and 20) and can be explained in terms of ordering of deuterium atoms in the "$ErFe_3$" interstitial sites of $ErFe_2$ (see Sec. III B 1).[19,21]

The outgassing of deuterium from $ErFe_2D_{3.2}$ powder commences at $\sim 160\,^{\circ}C$, as revealed by differential-scanning-calorimetry measurements of $ErFe_2D_{3.2}$ powder in an open sample pan: Above $\sim 160\,^{\circ}C$ the surface oxide of the powder breaks down, allowing deuterium to escape. Therefore, the deuterium can be kept in the solid during high-temperature measurements only by containing the powder in a closed cell. Application of the ideal gas law indicates that the pressure increase in such a cell for a loss of only 0.4 deuterium atoms per $ErFe_2$ formula unit can be 2×10^6 Pa (20 atm) or more.

For the DSC measurements deuterium was held in the sample by sealing the powder in a high-pressure DSC pan (Perkin-Elmer No. 0319-0218). The lid and base of the pan are constructed of 304 stainless steel and sealed together by a Viton O-ring, enabling the pan to withstand an internal overpressure of approximately 2.5×10^6 Pa (25 atm) up to $\sim 425\,^{\circ}C$, at which temperature the O-ring begins to decompose. The experimental protocol followed for each DSC scan was quite simple: after preannealing the 25-atm DSC pan bases and lids under vacuum to remove volatile surface impurities, from 10 to 100 mg of $ErFe_2D_{3.2}$ powder was sealed in a pan in a helium-filled glove bag. The sample was then scanned in the DSC using an empty 25-atm pan base+lid (without O-ring) as a reference. Scanning rates usually ranged from 5 to 20 °C, though some slower and faster scans were performed as part of a Kissinger analysis.

As with the DSC experiments, special procedures had to be followed in order to perform diffraction measurements on $ErFe_2D_{3.2}$ at elevated temperatures. The pressure increase associated with deuterium outgassing makes high-temperature x-ray diffraction quite difficult, since the candidate materials for making a sample enclosure—materials that scatter x rays only weakly, such as beryllium or other elements with low atomic number—are either structurally weak or difficult to machine into a leak-tight container. In contrast, neutrons, which have much smaller scattering cross sections than x rays and, consequently, longer penetration depths, place no serious restrictions on cell construction. The desire to study the structure of $ErFe_2D_{3.2}$ through the "λ-anomaly" temper-

ature of ~200 °C thus led us to perform elastic neutron diffraction on the deuterated powder enclosed in a stainless-steel sample cell with wall thickness 0.51 mm (0.020″).

The sample cell was heated by two resistance heating coils surrounding the upper and lower portions of the cell, the entire assembly of which was enclosed in a vanadium heat shield inside an aluminum vacuum chamber. Temperature measurement was made with a chromel-alumel (type-*K*) thermocouple in contact with the sample holder. The temperature could be maintained within ±2 °C of the setpoint, although initial overshoot was usually about 10 °C. For this reason, the temperature quoted for a neutron-diffraction measurement must be viewed as approximate. Fortunately, accurate transition temperatures could be determined using the DSC, for which precise temperature calibration is feasible.

We performed all of the elastic neutron-diffraction measurements on the powder diffractometer at the University of Missouri Research Reactor (MURR) utilizing neutrons of wavelength 0.154 720 nm and a position-sensitive detector arranged in Debye-Scherrer geometry covering a 2θ angular range of 20°. Approximately 850 mg of $ErFe_2D_{3.2}$ powder was sealed in the high-pressure stainless-steel sample holder under a helium atmosphere in a glove bag. Measurements were performed at progressively higher temperatures from ~70 to ~250 °C over an angular range of 35–75° 2θ. Bragg peaks arising from the stainless steel of the sample holder were identified by performing a scan of the empty sample holder. Neutron diffraction necessitated replacement of the hydrogen used in the experiment of Fecht *et al.* with deuterium in order to reduce the high background level caused by the nuclear spin incoherence of hydrogen.[22] Such a substitution should not have significantly influenced the results, however, since the isotope effect on the pressure-composition isotherms of hydrogenated $ErFe_2$ is known to be quite small.[23]

III. RESULTS

A. DSC measurements

Four signals were observed in sealed-pan DSC scans of $ErFe_2D_{3.2}$ from 35 to 400 °C (Fig. 1): two reversible, endothermic peaks with onset temperatures of approximately 90 and 200 °C and two irreversible, exothermic peaks with onsets at approximately 280 and 360 °C. The gradual increase in background seen in Fig. 1 is reversible and is caused by outgassing of a small amount of deuterium from the sample in order to maintain chemical equilibrium between the deuterium in the solid and gaseous phases. The first time that the temperature of a sample is scanned above ~160 °C (the temperature at which the surface oxide layer breaks down), the internal pressure in the DSC pan rises suddenly and causes a slight amount of deformation of the pan. The deformation of the pan is associated with a strong, irreversible, endothermic signal at about ~180 °C in the DSC that results from the outgassing of deuterium needed to reestablish chemical equilibrium in the newly deformed pan. Since the signals at

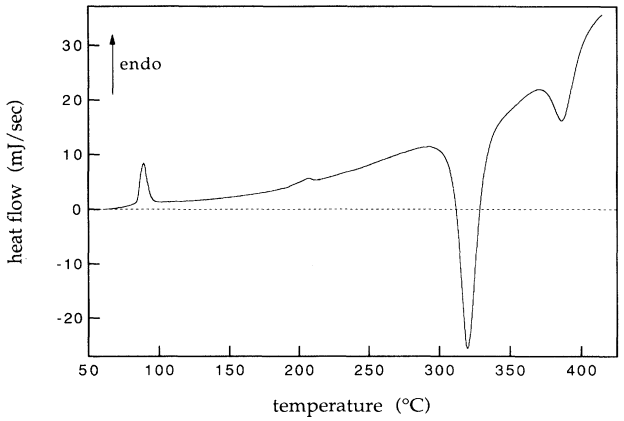

FIG. 1. DSC scan at 10°/min of $ErFe_2D_{3.2}$ sealed in a high-pressure, stainless-steel pan. The signal from the pan itself was removed by subtracting the signal from an empty pan scanned under identical conditions. The two endothermic signals are reversible, while the two exothermic signals are irreversible.

90 and 200 °C are reversible, this pan-deformation endothermic signal can be removed by heating the sample in the pan up to about 230 °C and then cooling to room temperature before performing the DSC measurement. Such a procedure breaks down the oxide layer that contains the deuterium in the solid, thus permitting the deuterium to enter and leave the sample at temperatures much below 160 °C. Not surprisingly, the background increase associated with outgassing is seen to begin around 70 °C in Fig. 1, for which the pan-deformation signal removal procedure was performed.

According to Kissinger,[24] the activation energy E_a of a single, thermally activated first-order transition seen in a DSC trace can be estimated from the dependence of the transition peak temperature T_p on scanning rate r according to the equation

$$\frac{d[\ln(r/T_p^2)]}{d[1/T_p]} = -\frac{E_a}{k_B} \ . \tag{1}$$

This expression is accurate only when the reaction is dominated by one thermally activated process with an Arrhenius temperature dependence. For a higher-order transition, which has no nucleation barrier, T_p will be independent of r; application of Eq. (1) to such a situation will result in unphysically high estimates of E_a. Kissinger plots for the two endothermic reactions seen in the DSC scans are shown in Figs. 2(a) and 2(b). The slope of the fitted straight line provides an estimate for E_a, and the error of the least-squares fits provides a measure of the statistical uncertainty in E_a. The apparent activation energies derived from such plots for the two endothermic transitions are unphysically high, suggesting that these transitions are not first order. The exothermic reaction at ~280 °C [Fig. 2(c)], on the other hand, has a reasonable activation energy of 1.02±0.04 eV/atom, although the deviation of the data points from a straight line suggests that one or more of the assumptions necessary for the validity of Eq. (1) have broken down. Hence, the

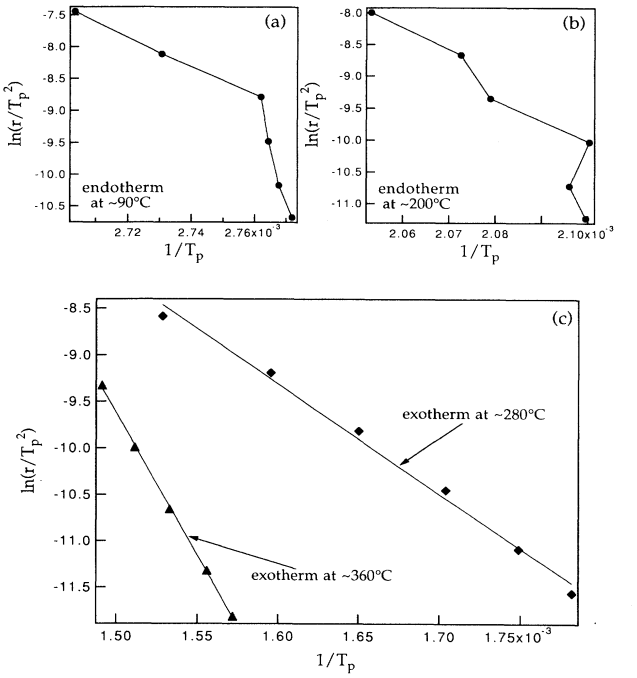

FIG. 2. Kissinger plots of $\ln(r/T_p^2)$ vs $1/T_p$ (K^{-1}) for the (a) endothermic signal at ~90 °C, (b) endothermic signal at ~200 °C, and (c) exothermic transitions at ~280 and ~360 °C. The scanning rate r ranged from 3°/min to 80°/min. T_p is the peak of the transition signal as measured in the DSC.

value derived for E_a should be viewed as only an approximation to the true value. The Kissinger analysis estimate of the activation energy for the exothermic signal at ~360 °C [Fig. 2(c)] is 2.65±0.04 eV/atom. In the discussion below (Sec. IV A) we shall discuss the proper interpretation of these activation energies in light of the atomic rearrangements occurring in both transitions.

B. Diffraction measurements

A combination of high-temperature neutron-diffraction measurements and room-temperature x-ray-diffraction measurements was performed to study the nature of each of the transitions identified in the DSC scan of Fig. 1.

1. Endothermic signal at ~90 °C

Elastic-neutron-diffraction scans below and above the endothermic peak at ~90 °C reveal than the crystalline structure changes from rhombohedral below the transition to cubic above it (Fig. 3 at 80 and 100 °C). We may understand such a rhombohedral-to-cubic transition in terms of a change in the interstitial site occupancy of deuterium atoms in the C15 Laves structure. As mentioned above, the rhombohedrally distorted room-temperature structure of $ErFe_2D_{3.2}$ results from ordering of deuterium atoms in "$ErFe_3$" interstitial sites,[19,21] the equivalence of which is broken by the loss of cubic symmetry. Above a certain temperature these deuterium atoms gain enough energy to jump between the various "$ErFe_3$" sites, thus occupying all of them with the same probability and forcing the lattice back into the cubic configuration. We conclude that the endothermic peak at ~90 °C results from a reversible order-disorder transition of the deuterium atoms in the "$ErFe_3$" sites of the C15 Laves structure. Since many such order-disorder transitions are second or higher order,[25] it is not surprising that the Kissinger analysis fails to provide a reasonable activation energy for the transition.

2. Endothermic signal at ~200 °C

Elastic-neutron-diffraction data reveal no structural change in the metal lattice of $ErFe_2D_{3.2}$ upon passing through the temperature range of this reversible peak (Fig. 3 at 165, 200, and 220 °C). The asymmetric shape of the DSC scan of this transition (Fig. 4) and the Kissinger analysis results suggest a higher-order phase transition—possibly another order-disorder transition of

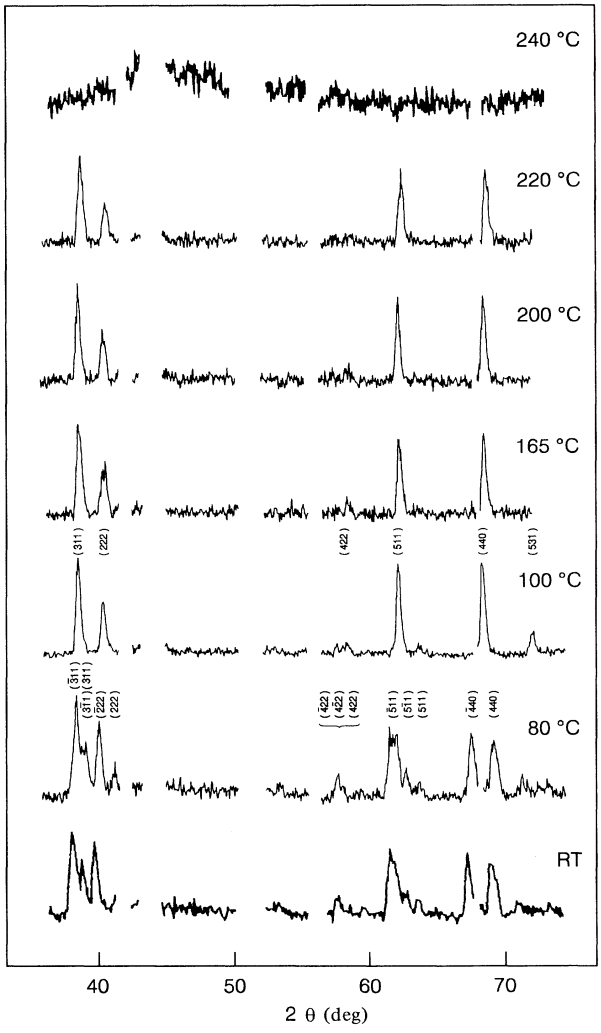

FIG. 3. Elastic-neutron-diffraction scans of $ErFe_2D_{3.2}$ performed at temperatures ranging from room temperature to 240 °C. Regions in the scans with no counts result from deletion of Bragg peaks from the stainless-steel sample holder.

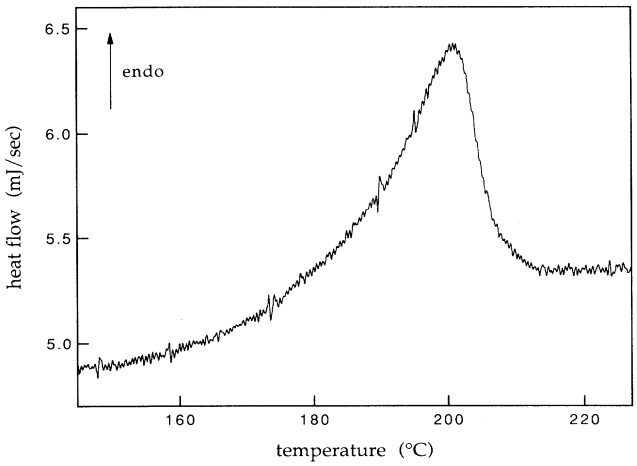

FIG. 4. DSC scan at 10°/min of the reversible transition at ~200 °C in $ErFe_2D_{3.2}$. Asymmetry suggests that the transition is not first order; the signal likely results from the Curie transition.

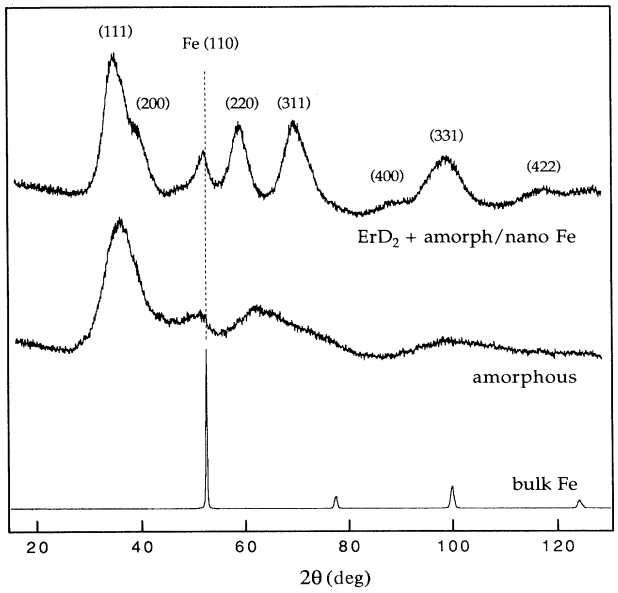

FIG. 5. X-ray-diffraction scans of $ErFe_2D_{3.2}$ heated above the exothermic signal at ~280 °C (middle) and above the exothermic signal at ~360 °C (top). Unlike the middle scan, the top scan has intensity maxima at the expected angles for ErD_2 (indexed diffraction peaks), indicating that ErD_2 has crystallized out of the amorphous phase. The peak at about 53° 2θ in both deuteride scans is close to, but slightly shifted from, the position of the bulk Fe(110) peak (bottom).

the deuterium atoms. It is more likely, however, that the signal results from the Curie transition of the cubic C15 structure formed at ~90 °C. Neutron-diffraction measurements on $ErFe_2D_x$ with $x \approx 3.5$ and C15 structure claimed to find a Curie transition temperature of 167 °C;[26] the same authors measured the Curie transition of unhydrogenated $ErFe_2$ to be 301 °C. Assuming as a first approximation that the Curie temperature depends linearly on x, we would expect to find the Curie transition of cubic $ErFe_2D_{3.2}$ at ~180 °C. Given the crude approximation inherent in this estimate and the uncertainty of the deuterium concentration in our sample at elevated temperature, the agreement appears to be rather good. Evidence of a change in the magnetic properties of the sample might have been derived from the neutron-diffraction data had our diffraction scan included the (111) Bragg peak at ~20° 2θ, since the contribution of scattering from the Fe magnetic moment to the integrated intensity of the (111) peak is stronger than its contribution to any other Bragg peak.[26] Unfortunately, our counting statistics were not good enough to detect the smaller magnetic contributions to the intensities of higher-angle peaks.

3. *Exothermic signal at ~280 °C*

The elastic-neutron-diffraction Bragg peaks of crystalline $ErFe_2D_{3.2}$ disappear irreversibly between 220 and 240 °C (Fig. 3). Upon cooldown to room temperature, x-ray-diffraction scans of the powder from the neutron measurement revealed no Bragg peaks—only an intensity signal characteristic of that of an amorphous structure (Fig. 5). X-ray-diffraction scans of $ErFe_2D_{3.2}$ cooled to room temperature after having been heated in the DSC above the irreversible, exothermic transition at ~280 °C were identical to those from the neutron-diffraction experiment. Thus, we associate the first exothermic signal with amorphization of the sample.

The discrepancy in the amorphization onset temperatures found in the neutron-diffraction and DSC measurements ($\Delta T \approx 50$ °C) arises primarily from the time delay in the scanning experiment caused by the activation energy of the process. This conclusion follows from a simple scaling argument. Assuming a characteristic length L over which diffusion occurs for the amorphization transition to occur (see Sec. IV A), we know from the units of the diffusion coefficient D that $L \propto \sqrt{D(T)t(T)}$, where diffusion occurs at temperature T for a time t. Using the standard empirical expression for D $[D = D_0 \exp(-E_a/k_B T)]$, we can express the temperature difference $\Delta T = T_2 - T_1$ in terms of the times $t(T_2)$ and $t(T_1)$ for diffusion to occur over L at the respective temperatures:

$$\frac{\Delta T}{T_1 T_2} = \frac{k_B}{E_a} \ln \left[\frac{t(T_1)}{t(T_2)} \right] . \tag{2}$$

The measured ΔT is consistent with $t(T_1)$ (~30 min during neutron-diffraction measurement), $t(T_2)$ (~3 min in the DSC), and the E_a value for amorphization (1 eV/atom) determined from the Kissinger analysis.

The enthalpy release upon heating through the amorphization transition, obtained by integrating the area of the exothermic peak, is ~6.7 kJ/(mole of atoms),[27] which is comparable in magnitude to the 5–9 kJ/(mole of atoms) heat of fusion that one would estimate using Richard's rule[28] for melting of the crystal at the amorphization temperature. As mentioned in the Introduction, chemical analysis reveals a change in (room-temperature) deuterium concentration from $ErFe_2D_{3.2}$ in

the crystalline phase to $ErFe_2D_{2.8}$ in the amorphous phase, which is in good agreement with the composition of amorphous hydrogenated $ErFe_2$ formed directly by annealing $ErFe_2$ in a hydrogen atmosphere at 240 °C.[17]

4. *Exothermic signal at ~360 °C*

No neutron-diffraction scans were recorded above 250 °C, but the structural changes associated with the exothermic signal at ~360 °C could be determined from room-temperature x-ray-diffraction scans of samples heated through the transition because it is irreversible. While such scans reveal rather broad intensity maxima similar to those of the sample after amorphization, they can be indexed to the expected Bragg peaks of ErD_2 and also, perhaps, to Fe (Fig. 5). The precipitation of ErD_2 should leave behind Fe-rich clusters, but only a peak near the strong (110) Fe position is obvious in the diffraction scan; there are none corresponding to Fe reflections at higher angles. Even the possible Fe (110) peak is noticeably displaced from its position in bulk Fe, though this could reflect lattice expansion due to interstitial D or to alloying with Er. Analysis of a similar crystalline hydride, $GdFe_2H_{4.2}$, in a high-pressure differential thermal analyzer (DTA) by Aoki, Li, and Masumoto found separate exothermic signals corresponding to precipitation of GdH_2 and Fe.[29] This suggests by analogy that ErD_2 crystallizes out of amorphous $ErFe_2D_{2.8}$ at ~360 °C, leaving the Fe in an amorphous phase whose apparent "(110)" peak is actually the usual nearest-neighbor intensity maximum. Unfortunately, crystallization of the Fe regions did not occur at a low enough temperature (i.e., below 425 °C) to enable identification of the corresponding DSC signal. Application of the Scherrer formula[30] for the effect of small grain size on peak width suggests that the crystallized ErD_2 grain size L is quite small:

$$L \approx \frac{0.9\lambda}{B\cos\theta_B} \approx 2 \text{ nm} , \tag{3}$$

where λ is the x-ray radiation wavelength and B is the full width at half maximum of the diffraction peak at $2\theta_B$.

IV. DISCUSSION

A. Exothermic amorphization

As discussed in the Introduction, hydrogen-induced amorphization of a crystalline intermetallic compound should be a polymorphous transformation because it occurs at low temperatures where the metal atoms lack the necessary mobility to phase separate. If HIA occurs in response to an underlying instability of the crystalline phase, then the general polymorphous phase diagram of Fecht and Johnson[11] would predict the amorphization transformation to occur reversibly at the temperature at which the solid and amorphous phases have the same free energy, i.e., where $\Delta G = 0$. This latter equation implies that at the amorphization temperature T_a, $\Delta H = T_a \Delta S$, the right-hand side of which is clearly greater than zero because of the increase in configurational entropy when transforming from the crystalline to the amorphous state. Thus, if HIA is a polymorphous melting process in the sense of the Fecht-Johnson diagram, such amorphization should be both reversible and endothermic.

In contrast to these expectations, the DSC and neutron experiments described above indicate that HIA of $ErFe_2$ is irreversible and exothermic. Convincing evidence that HIA of rare-earth–Fe_2 compounds is, in general, an exothermic process was recently obtained by Aoki and coworkers using high-pressure differential thermal analysis.[15,29,31] In the case of $ErFe_2$ deuteride, such a result can be understood from an analysis of the change in the atomic-level structure of the sample during the amorphization transition. The majority of information that we have about the amorphous phase is found in its x-ray-diffraction scan (Fig. 6), which has an unusual amount of structure for a diffraction scan of an amorphous solid. To first approximation we can attempt to understand the origin of the peaks in the scan by asking if the low-angle intensity maxima in the amorphous diffraction scan correspond to reasonable nearest-neighbor interatomic distances in the solid. For an intensity maximum centered on a diffraction angle $2\theta_m$, the corresponding interatomic spacing d_m is given by Ehrenfest's formula:[32]

$$d_m = K\frac{\lambda}{2\sin\theta_m} , \tag{4}$$

where λ is the wavelength of x-ray radiation and K is a constant equal to 1.1–1.2. Keeping in mind that the assumptions made in deriving this formula render it useful only for rough predictions in most cases,[32,33] we get distances of $d_m \approx 0.35$ nm for the lowest-angle maximum and $d_m \approx 0.25$ nm for the next-highest-angle maximum in Fig. 6. In $ErFe_2$, the Fe—Fe bond distance is 0.257 nm, Er—Fe is 0.301 nm, and Er—Er is 0.314 nm.[34] It is tempting to associate the first intensity maximum with the Er—Er bond length and the second with the Fe—Fe bond length. These peaks can be distinguished only if the amorphous phase has relatively few Er—Fe nearest neighbors; otherwise, overlap with the signal from Er—Fe bonds—which would fall between the other two maxima—would result in one broad intensity maximum in the diffraction scan. That the amorphous solid has relatively few Er—Fe nearest neighbors strongly implies the existence of short-range clustering of Er and Fe atoms with other atoms of the same kind.

This clustering explanation for the structure of the amorphous diffraction scan has been placed on a firm foundation by comparison of the radial distribution function (RDF) of amorphous $ErFe_2$ with that of hydrogenated amorphous $ErFe_2$.[34,35] The difference in partial coordination numbers between crystalline $ErFe_2$ and amorphous hydrided $ErFe_2$ provides evidence for almost complete clustering of Er and Fe atoms with like neighbors: the partial correlation number of Fe—Er drops from 6 in the crystal to 1.1 in the hydrogenated glass. It is no surprise, then, that a contribution to the nearest-neighbor

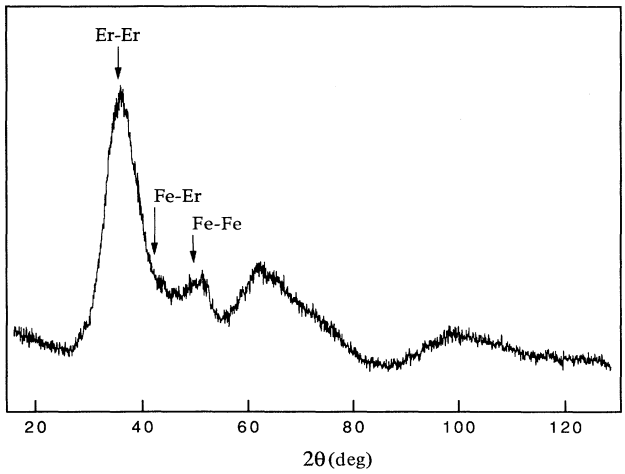

FIG. 6. X-ray scan of amorphous $ErFe_2D_{2.8}$. The unusual split first-intensity maximum can be identified with Er—Er and Fe—Fe nearest-neighbor interatomic spacings, while the lack of intensity between these peaks can be attributed to a dearth of Fe—Er nearest neighbors in the amorphous structure. Intensity maxima positions were predicted using Ehrenfest's formula [Eq. (4)].

amorphous peak from Fe—Er interatomic distances is missing from the x-ray-diffraction scan.

The large enthalpy release associated with amorphization can be seen to arise from the change in local environment of the deuterium atoms in the solid. Instead of having at most two Er nearest neighbors—to which an interstitial deuterium atom is limited in the C15 crystalline structure[19]—the deuterium atoms in the amorphous phase can surround themselves almost entirely with Er atoms by occupying interstitial sites in and around the Er-rich regions. The clustering enables the deuterium atoms to avoid energetically unfavorable Fe neighbors. The enthalpy release gained from this favorable change in deuterium environment provides the energy to drive the atomic-level decomposition of the crystalline $ErFe_2D_{3.2}$ phase that results in amorphization. The driving force for hydrogen-induced amorphization has long been attributed to the energetically advantageous hydrogen environments present in the amorphous phase;[36] here we have succeeded in directly measuring the sizable enthalpy release associated with amorphization from an already-hydrogenated crystalline state.

The activation energy measured by the Kissinger method should be consistent with this model for the amorphization process. The activation energy $E_a \approx 1.0$ eV/atom for amorphization of $ErFe_2D_{3.2}$ must correspond to the barrier hindering atomic rearrangement from the C15 Laves phase of crystalline $ErFe_2D_{3.2}$ to the clustered amorphous state of $ErFe_2D_{2.8}$. The change in atomic configuration found in the RDF analysis requires some diffusion of metal atoms to occur. We expect Fe atoms to diffuse much more rapidly in $ErFe_2D_{3.2}$ than Er atoms because the Fe atoms are much smaller than the Er atoms. While there are no known measurements of the activation energy for Fe diffusion in $ErFe_2D_{3.2}$ [Goldschmidt radius $r_{Fe}=0.126$ nm (Ref. 37)] or even in bulk Er ($r_{Er}=0.175$ nm), we can get a rough idea of its value from the measured E_a for the diffusion of Au ($r_{Au}=0.144$ nm) in Er: 0.66 eV/atom parallel to the c axis of Er and 1.0 eV/atom perpendicular to it.[38] The activation energy for Au diffusion in $ErFe_2D_{3.2}$ would probably be higher than in pure Er, since the "average metal atom" is smaller in $ErFe_2D_{3.2}$, but Fe atoms are smaller than Au atoms, which would tend to lower the activation energy, so it is reasonable to assign the activation energy $E_a \approx 1.0$ to Fe diffusion. Thus, the onset temperature of the amorphization process is the temperature at which the Fe atoms can diffuse away from their Er neighbors, permitting the deuterium atoms to surround themselves primarily with Er atoms.

The activation energy for crystallization of ErD_2 in amorphous $ErFe_2D_{2.8}$ determined by the Kissinger analysis is $E_a \approx 2.7$ eV/atom. This value is much higher than the E_a for amorphization, which implies that a different mechanism governs crystallization of ErD_2. It is reasonable to assume that a certain amount of atomic rearrangement in the Er+D cluster will be necessary for crystallization to occur. Therefore, the measured activation energy may correspond to Er diffusion, which would likely be the rate-limiting step in the crystallization process; not surprisingly, the measured activation energy for ErD_2 crystallization is close to that of Er self-diffusion [3.1 eV/atom (Ref. 39)].

That this model for HIA may be applicable to intermetallic compounds other than $ErFe_2$ is supported by the DTA measurements of Aoki, Li, and Masumoto on $GdFe_2H_{4.2}$,[29] which has a C15 Laves structure like that of $ErFe_2D_{3.2}$ (above the order-disorder transition). The activation energies for amorphization (1.2 eV/atom) and for crystallization of GdH_2 (2.1 eV/atom) that they derived from the Kissinger analysis technique were quite similar to those we obtained for the corresponding transitions in $ErFe_2D_{3.2}$ (1.0 eV/atom and 2.7 eV/atom, respectively).

B. Violation of the polymorphous constraint

The clustering of Er and Fe during amorphization of $ErFe_2D_{3.2}$ occurs without apparent phase separation, at least as phase separation is traditionally considered, since the clusters of Er and Fe are probably as small as or even smaller than the ~2-nm ErD_2 regions that crystallize at a higher temperature. Thus, the amorphization reaction is essentially polymorphous, except when considered at an almost atomic length scale. The fact that amorphization of $ErFe_2D_{3.2}$ occurred irreversibly and exothermically, in direct contradiction to the predictions of the Fecht-Johnson polymorphous phase diagram, suggests that an actual instability-induced collapse of a crystalline phase can only be experimentally realized in systems in which phase separation is avoided at all length scales—including the very short ones at which phase separation is better described as clustering. The prospects for finding such a system among those that undergo HIA are poor, since all known compounds that undergo HIA are

made up of both good and poor hydride-forming elements. Preferential chemical bonding (between the good hydride formers and hydrogen) is likely to induce short-range clustering in all HIA systems, and, in fact, the tendency to short-range order is the likely underlying cause of all instances of hydrogen-induced amorphization.

C. Is the "λ anomaly" associated with amorphization?

The DSC and neutron-diffraction measurements described above make it highly unlikely that the apparent "λ anomaly" in the DSC trace of $ErFe_2H_{3.4}$ seen by Fecht, Fu, and Johnson[17] is related to a reversible amorphization reaction. Not only was (irreversible) amorphization found in the high-temperature neutron-diffraction experiments at a temperature at least 30 °C above that of the "λ anomaly," but the signal from the deformation of the stainless-steel DSC pan, which was found at about the same temperature as the "λ anomaly," would be expected to occur in response to a much higher internal pressure than the 2×10^5 Pa (2 atm) rating of the sealed aluminum pans used by Fecht *et al.* That is, their pans could not have remained intact upon heating through the deformation-induced endothermic transition that we observed at ~200 °C because their seals would have broken once a small amount of outgassing from the powder had occurred.

In fact, it is reasonable to suppose that the "λ anomaly" is simply the deformation peak of the sealed aluminum pans: the low-temperature edge of the signal would rise for the same reasons as with the deformation peak of the stainless-steel pans (gas evolution from the sample necessary for maintaining chemical equilibrium; see Sec. III A) and the quick dropoff on the high-temperature side might result from a sudden ceasing of the deformation. That is, the deformation of the aluminum pan might proceed rapidly until reaching a point at which further deformation could only occur by breaking the seal, a process that may require significantly more internal pressure than that needed for the initial deformation. Indeed, several scans of $ErFe_2D_{3.2}$ in the same sealed aluminum DSC pans used by Fecht *et al.* produced "λ-like" signals just before seal failure.

We must also question the finding by Fecht *et al.* of amorphous regions in TEM images of $ErFe_2H_{3.4}$ heated through the "λ anomaly" and subsequently cooled to room temperature. We saw no amorphous regions in x-ray-diffraction scans of $ErFe_2D_{3.2}$ heated up to the onset of the exothermic amorphization DSC signal. Perhaps the amorphous regions seen by Fecht *et al.* were an artefact of TEM sample preparation or were caused by the influence of the electron beam and degassing of the sample in the microscope.

V. CONCLUSIONS

Hydrogen-induced amorphization of $ErFe_2$ is a non-polymorphous transformation driven by the clustering of hydrogen atoms around the good hydride-forming Er atoms. It was not possible to realize a polymorphous variant of HIA in this system by maintaining a nearly constant hydrogen concentration through the transition. Reversible, endothermic amorphization, as expected of instability-induced amorphization, is not observed in HIA because the loss of long-range crystalline order results from short-range clustering of atoms rather than from a polymorphous collapse of the crystalline state. Therefore, the speculation of Fecht, Fu, and Johnson[17] that the "λ anomaly" seen in DSC measurements of $ErFe_2H_{3.4}$ is associated with reversible amorphization cannot be true. Such an anomalous signal more likely arose from deformation of the sealed DSC pans in response to the buildup of internal pressure resulting from hydrogen outgassing from the sample.

ACKNOWLEDGMENTS

We are grateful to the staffs of MURR and of the machine shop of the Department of Physics at the University of Missouri-Columbia for their expert assistance. It is a pleasure to acknowledge useful discussions with Dr. Z. Fu, Dr. R. Birringer, and Professor H. J. Fecht. Financial support for these experiments came from the U.S. Department of Energy under Contract Nos. DE-FG05-89ER75511 (x-ray-diffraction measurements) and DE-FG03-86ER25242.

*Present address: FB 15 Werkstoffwissenschaften, Gebäude 43, Universität des Saarlandes, Postfach 1150, D-66041 Saarbrücken, Germany.

[1]W. L. Johnson, Prog. Mater. Sci. **30**, 81 (1986).
[2]X. L. Yeh, K. Samwer, and W. L. Johnson, Appl. Phys. Lett. **42**, 242 (1983).
[3]D. E. Luzzi, H. Mori, H. Fujita, and M. Meshii, Acta Metall. **34**, 629 (1986).
[4]D. Wolf, P. R. Okamoto, S. Yip, J. F. Lutsko, and M. Kluge, J. Mater. Res. **5**, 286 (1990).
[5]D. E. Luzzi, J. Mater. Res. **6**, 2059 (1991).
[6]P. R. Okamoto and M. Meshii, in *Science of Avanced Materials,* edited by H. Wiedersich and M. Meshii (American Society for Metals, Metals Park, OH, 1990), pp. 33–98.
[7]G. Linker, Solid State Commun. **57**, 773 (1986).
[8]A. Seidel, S. Massing, B. Strehlau, and G. Linker, Phys. Rev. B **38**, 2273 (1988).
[9]C. E. Krill III, J. Li, C. Ettl, K. Samwer, W. B. Yelon, and W. L. Johnson, J. Non-Cryst. Solids **156-158**, 506 (1993).
[10]W. L. Johnson, M. Li, and C. E. Krill III, J. Non-Cryst. Solids **156-158**, 481 (1993); M. Li and W. L. Johnson, Phys. Rev. Lett. **70**, 1120 (1993).
[11]H. J. Fecht and W. L. Johnson, Nature (London) **334**, 50 (1988).
[12]H. J. Fecht, Nature (London) **356**, 133 (1992).
[13]R. C. Bowman, Jr., J. S. Cantrell, K. Samwer, J. Tebbe, E. L. Venturi, and J. J. Rush, Phys. Rev. B **37**, 8575 (1988).
[14]K. Aoki, X.-G. Li, T. Aihara, and T. Masumoto, Mater. Sci. Eng. A **133**, 316 (1991).
[15]K. Aoki, A. Yanagitani, X.-G. Li, and T. Masumoto, Mater.

Sci. Eng. **97**, 35 (1988).
[16]U.-I. Chung, Y.-G. Kim, and J.-Y. Lee, Philos. Mag. B **63**, 1119 (1991).
[17]H. J. Fecht, Z. Fu, and W. L. Johnson, Phys. Rev. Lett. **64**, 1753 (1990).
[18]B. D. Cullity, *Elements of X-ray Diffraction,* 2nd ed. (Addison-Wesley, Menlo Park, CA, 1978), p. 511.
[19]J.-M. Park and J.-Y. Lee, Scr. Metall. **23**, 1525 (1989).
[20]T. de Saxcé, Y. Berthier, and D. Fruchart, J. Less-Common Met. **107**, 35 (1985).
[21]D. Fruchart, Y. Berthier, T. de Saxcé, and P. Vuillet, J. Less-Common Met. **130**, 89 (1987).
[22]G. Kostorz and S. W. Lovesey, in *Treatise on Materials Science and Technology,* edited by G. Kostorz (Academic, New York, 1979), Vol. 15, pp. 4–8.
[23]T. B. Flanagan, J. D. Clewley, N. B. Mason, and H. S. Chung, J. Less-Common Met. **130**, 309 (1987).
[24]H. E. Kissinger, Anal. Chem. **29**, 1702 (1957).
[25]A. H. Cottrell, *An Introduction to Metallurgy* (Arnold, London, 1967), p. 220.
[26]G. E. Fish, J. J. Rhyne, S. G. Sankar, and W. E. Wallace, J. Appl. Phys. **50**, 2003 (1979).
[27]This area is not exactly equivalent to ΔH because the pressure inside the sealed pan is not constant during the transition. Unfortunately, there is no easy way to measure the pressure change in the DSC pan.
[28]D. R. Gaskell, in *Physical Metallurgy,* 3rd ed., edited by R. W. Cahn and P. Haasen (Elsevier, Amsterdam, 1983), Part 1, p. 278.
[29]K. Aoki, X.-G. Li, and T. Masumoto, Acta Metall. Mater. **40**, 221 (1992).
[30]B. D. Cullity, *Elements of X-ray Diffraction,* 2nd ed. (Addison-Wesley, Menlo Park, CA, 1978), p. 102.
[31]K. Aoki, A. Yanagitani, and T. Masumoto, Appl. Phys. Lett. **52**, 2122 (1988).
[32]A. Guinier, *X-Ray Diffraction in Crystals, Imperfect Crystals, and Amorphous Bodies* (Freeman, San Francisco, 1963), p. 73.
[33]H. P. Klug and L. E. Alexander, *X-ray Diffraction Procedures for Polycrystalline and Amorphous Materials,* 2nd ed. (Wiley, New York, 1974), pp. 847–850.
[34]M. Matsuura, K. Fukamichi, H. Komatsu, K. Aoki, T. Masumoto, and K. Suzuki, Mater. Sci. Eng. **97**, 223 (1988).
[35]For the RDF measurements of Ref. 34, the hydrogen-containing amorphous phase was obtained by hydrogenating an *already amorphous* film of $ErFe_2$ rather than by inducing a crystal-to-amorphous phase transition in the crystalline hydride, as we did with $ErFe_2D_{3.2}$. Both techniques should lead to the same amorphous structure, however, since—as mentioned in the Introduction—comparative studies of hydrogenation of amorphous and crystalline Zr_3Rh found no significant structural differences in the final states (Refs. 2 and 13).
[36]K. Samwer and W. L. Johnson, Phys. Rev. B **28**, 2907 (1983).
[37]*Smithells Metals Reference Book,* 6th ed., edited by E. A. Brandes (Butterworths, Boston, 1983), pp. 4-25–4-28.
[38]M. P. Dariel, L. Kornblit, B. J. Beaudry, and K. A. Gschneidner, Phys. Rev. B **20**, 3949 (1979).
[39]F. H. Spedding and K. Shiba, J. Chem. Phys. **57**, 612 (1972).